A neuroevolution potential for predicting the thermal conductivity of α, β, and ε-Ga_2O_3

Zhanpeng Sun [a, d, #], Zijun Qi [a, d, #], Kang Liang [a, b, d], Xiang Sun [a, b, d], Zhaofu Zhang [a], Lijie Li [c], Qijun Wang [a, d], Guoqing Zhang [a], Gai Wu [a, b, d, *], Wei Shen [a, b, d, e, **]

[a] *The Institute of Technological Sciences, Wuhan University, Wuhan 430074, China*

[b] *School of Power and Mechanical Engineering, Wuhan University, Wuhan, 430072, China*

[c] *College of Engineering, Swansea University, Swansea, SA1 8EN, UK*

[d] *Wuhan University Shenzhen Research Institute, Wuhan University, Shenzhen, 518057, China*

[e] *Hubei Key Laboratory of Electronic Manufacturing and Packaging Integration, Wuhan University, Wuhan, 430072, China*

Corresponding Authors:

[*]*Gai Wu, E-mail: wugai1988@whu.edu.cn*

[**]*Wei Shen, E-mail: wei_shen_@whu.edu.cn*

[#]*Zhanpeng Sun and Zijun Qi contributed equally to this work.*

ABSTRACT

Ga_2O_3 is an ultrawide-bandgap semiconductor with a variety of crystal configurations, which has the potential for a variety of applications, especially in power electronics and ultraviolet optoelectronics. However, there has been no single interatomic potential reported for Ga_2O_3 polymorphs in terms of molecular dynamics prediction of thermal conductivity. Here, one interatomic potential has been developed based on neural networks, which has the clear advantages of consuming less computational power than density functional theory and has high accuracy in predicting the thermal conductivity of the three polymorphs of Ga_2O_3. Using the neuroevolution potential, the thermal conductivity values at 300 K have been predicted. Hence, the $\kappa_{[average-\alpha]}$ was 67.2% that of β-Ga_2O_3, and the $\kappa_{[average-\varepsilon]}$ was only 26.4% that of β-Ga_2O_3. The possible reasons for the discrepancies in thermal conductivity values in various crystal types and orientations have been explored. As a result, it could be shown that the contribution of low-frequency phonons to thermal conductivity was very significant in Ga_2O_3, and a unit cell with low symmetry and high atomic number would

negatively impact the thermal conductivity of the material. In this work, a scheme has been proposed for accurately predicting the thermal conductivity of Ga_2O_3 and a relatively accurate value of the thermal conductivity of ε-Ga_2O_3 has been achieved, which could also provide an atomic-scale perspective for the insight into the thermal conductivity differences among α, β, and ε-Ga_2O_3.

Emerging as an ultrawide-bandgap semiconductor (UWBG), Ga_2O_3 has received much attention from the scientific community based on its large bandgap and high breakdown voltage.[1] Compared with traditional semiconductor materials such as Si, GaN, and SiC, Ga_2O_3 has a bandgap that exceeds 4.5 eV and a high breakdown electric field of ~9 $MV \cdot cm^{-1}$.[2-4] Ga_2O_3 is widely regarded as a promising semiconductor that can withstand large voltages, making it attractive for high-power devices.[5] However, due to the excessive heat generated with high power, there have been significant challenges in maintaining the stability of high-power devices made of Ga_2O_3.[6] The thermal conductivity of Ga_2O_3 is very low, such as $\kappa_{[average-\beta]}$ of ~15 $W \cdot m^{-1} \cdot K^{-1}$.[7] Ga_2O_3 has five polymorphs: α, β, γ, δ, and ε(κ).[8] The formation energy of these phases is in the order of $\beta < \varepsilon < \alpha < \delta < \gamma$,[9] among which β-$Ga_2O_3$ is the stable phase and ε-Ga_2O_3 and α-Ga_2O_3 are metastable phases. All the three stable and metastable phases are widely used in high-power devices.[10-12] Therefore, the investigation of the thermal conductivity of the Ga_2O_3 polymorphs, especially for the α, β, and ε-Ga_2O_3 phases, is in urgent need to optimize the performances of these polymorphs in device applications.

In the previous studies, the thermal conductivity measurements of Ga_2O_3 have primarily focused on the β phase, using the 2ω and 3ω methods and the time-domain thermoreflectance (TDTR) measurements.[13-17] More recently, Raman thermometry has also been utilized to study the thermal conductivity of β-Ga_2O_3 nanofilms and thin films.[18, 19] However, there are few specific reports regarding thermal conductivity measurements of the α and ε-phases. At present, numerical simulation studies have concentrated on two methods for the calculation of thermal conductivity. One is based on the density functional theory (DFT),[20-22] and the other uses the molecular dynamics (MD) simulations with empirical potentials.[23-25] Nevertheless, due to the large time and length scales required for heat transport processes, DFT methods require extensive computational resources, thus posing an application bottleneck for simulating the heat transport characteristics. Vilquin et al.,[26] Santia et al.,[20] and Zhou et al.[27] applied the DFT method to calculate the thermal conductivity of α, β and ε-Ga_2O_3, respectively. However, the results have yet to be verified. Simple empirical potential

simulation is orders of magnitude faster than the DFT approach,[28] but the desired level of precision for Ga_2O_3 is considerably higher than that provided using simple empirical potentials. Additionally, constructing such an empirical potential is a challenging task that requires considerable time and effort.[29] Thus, for the moment, there is no conventional potential for Ga_2O_3 that can be used to predict the thermal conductivity.

Recent research efforts have focused on machine learning (ML) to predict thermal conductivity.[30] In this approach, the ab *initio* potential energy surface is reconstructed via ML to obtain a highly precise interatomic potential, especially for the neuroevolution potential (NEP).[31] Utilizing the ML potential, other groups have recently confirmed the thermal conductivity of Si,[32] Zr,[33] graphene,[34] and MoS_2[35] at a computational speed comparable to or even faster than classical MD simulations and with an accuracy comparable to that of DFT. Some have used ML-potential (MLP) to calculate the thermal conductivity of β-Ga_2O_3. However, to date, few have used this approach to calculate the thermal conductivity of the α and ε phases nor compared the three phases.

In this work, the ability of the NEP based on ML has been demonstrated for the accurate prediction of lattice thermal conductivity of α-Ga_2O_3, β-Ga_2O_3, and ε-Ga_2O_3. Furthermore, a detailed analysis of the thermal conductivity differences among different phases of Ga_2O_3 has been conducted. As a result, it has been proven that the proposed approach based on ML-NEP is not only faster than that involving DFT calculations but with comparable accuracy, and could effectively address the issues of the lack of related potential functions in calculating the thermal conductivity of Ga_2O_3 via MD. Furthermore, a more accurate and reliable value of the thermal conductivity for ε-Ga_2O_3 has been achieved. In general, the great potential of the proposed ML-NEP strategy has been shown in predicting the thermal conductivity of Ga_2O_3 polymorphs in this work, potentially paving the way for a further understanding of the thermal properties of different Ga_2O_3 phases.

The ab *initio* molecular dynamics (AIMD) was used to obtain the α-Ga_2O_3, β-Ga_2O_3, and ε-Ga_2O_3 MD trajectories via the Vienna Ab Initio Simulation Package (VASP).[36, 37] Training data were constructed from these trajectories that were then applied to generate the MLP-NEP using Graphics Processing Units Molecular Dynamics code (GPUMD).[38-40] Finally, the generated NEP was used to calculate the lattice thermal conductivity of α-Ga_2O_3, β-Ga_2O_3, and ε-Ga_2O_3 based on the equilibrium molecular dynamics (EMD) method.

As shown in Fig. 1, Corundum structure α-Ga_2O_3 has a $R\bar{3}c$ crystal symmetry,[41] in which each

conventional unit cell contains 18 gallium atoms and 12 oxygen atoms. Monoclinic structure β-Ga_2O_3 has a *C2/m* crystal symmetry,[42] and each conventional unit cell includes 8 gallium atoms and 12 oxygen atoms. The orthorhombic structure ε-Ga_2O_3 has a *Pna21* crystal symmetry, and each conventional unit cell has 16 gallium atoms and 24 oxygen atoms. (In this work, cell structures all have been visualized utilizing VESTA software.[43]). In the training database, α-Ga_2O_3, β-Ga_2O_3, and ε-Ga_2O_3 comprised with 360, 320, and 320 atoms, respectively. A time step of 1 fs was used and the temperature was fixed at 600 K. As the training data that included structures at high temperatures could accurately predict the thermal properties at low temperatures,[44] the temperature gradient was not set in the training data in order to minimize the computational resources.

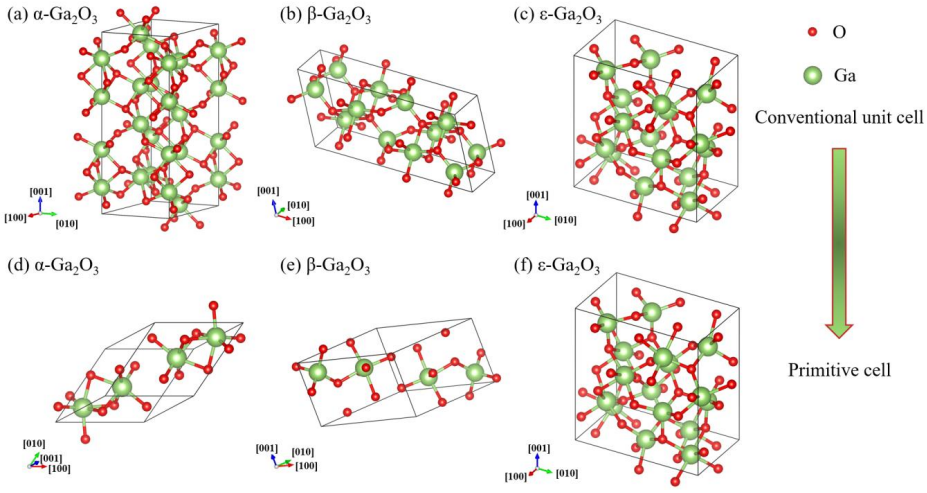

Fig. 1 Conventional unit cell of (a) α-Ga_2O_3, (b) β-Ga_2O_3, and (c) ε-Ga_2O_3 crystals, and primitive cell of (d) α-Ga_2O_3, (e) β-Ga_2O_3, and (f) ε-Ga_2O_3 crystals, respectively.

The NEP has three layers: the input layer, the hidden layer, and the output layer, which could be seen in Fig. S1 in the ***supporting information***. The potential energy surface function U_i for atom *i* in the NEP model is derived from the descriptor vector q_v^i, which can be determined by the following formula[31, 45, 46]:

$$U_i = \sum_{\mu=1}^{N_{neu}} \omega_\mu^{(1)} \tanh\left(\sum_{v=1}^{N_{des}} \omega_{\mu v}^{(0)} q_v^i - b_\mu^{(0)}\right) - b^{(1)} \quad (1)$$

where $tanh(x)$ is the activation function of the hidden layer, N_{des} is the number of components of the descriptor vector, N_{neu} is the number of neurons, $\omega^{(0)}$ is the matrix of connection weights from the

input layer to the hidden layer, $\omega^{(1)}$ is the vector of connection weights from the hidden layer to the output layer node U_i, $b^{(0)}$ is the bias vector of the hidden layer, and $b^{(1)}$ is the bias of the output layer node U_i. Compared to other machine learning algorithms, the NEP boasts high computational accuracy and efficiency in atomistic simulations and application to heat transport[45], which could greatly reduce the time cost and the dependence on large amounts of computational resources.

EMD simulations were used to evaluate the thermal conductivity based on the Green–Kubo approach.[47-49] The Green–Kubo formula relates the instantaneous fluctuations in heat current to thermal conductivity based on the autocorrelation function, as follows:[50]

$$k_\alpha(t) = \frac{1}{k_B T^2 V}\int_0^{t_0} < J_\alpha(0) J_\alpha(t) > dt \quad (2)$$

where, k_α represents the thermal conductivity in the α direction, k_B is the Boltzmann constant, V is the volume of the model cell, T is the temperature, t_0 is the integral upper limit, which should theoretically be infinite, J_α is the component of heat current J in the α direction, and $< >$ represents the ensemble average.

The bulk of the α-Ga_2O_3, β-Ga_2O_3, and ε-Ga_2O_3 included 9720, 9600, and 9000 atoms (at least 4.5 nm long in each crystallographic direction and at least 9000 atoms in each bulk). The model size of this work was more than 120% that of the previous similar works.[51, 52] Therefore, the convergence of the size is not proven again here. To reduce the calculation errors, 50 independent MD runs were performed to obtain the average κ values at 200~600 K.

Table 1 The NEP training hyperparameters.

Keywords	Parameters
type	2 Ga O
cutoff	6 4
n_max	10 8
basis_size	10 8
l_max	4 2
neuron	60
lambda_1	0.05
lambda_2	0.05
lambda_e	1.0
lambda_f	1.0
lambda_v	0.1
batch	3000
generation	180000

The training hyperparameters could be shown in Table 1. The loss terms for energy, force, and

virial relations in the test and training sets presented great convergence after 180,000 generations [Fig. 2(a)]. Parity plots of the energies, atomic forces, and atomic virial relations predicted from the NEP have been given in Fig. 2(b–d), showing good correlations. The root-mean-squared-error (RMSE) of the predictions for each plot has also been reported. Generally, the RMSE values of each trained MLP fell in the range of several meV/atom in energy and several hundred meV/Å in force, thus indicating satisfactory training.[53]

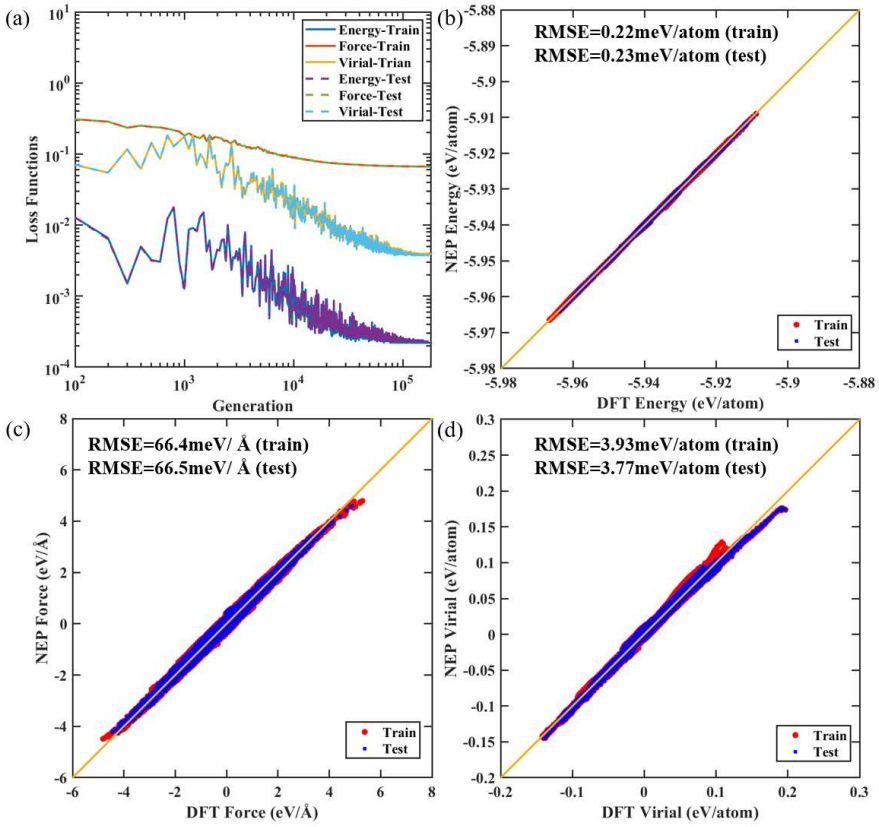

Fig. 2 (a) Loss function of energy, force, and virial for the training and test sets. (b)–(d) Comparison between the NEP predictions and DFT reference values of energy, force, and virial for the training and test sets, respectively.

Figure 3(a) shows the average integral of heat flow autocorrelation functions along the three crystallographic directions for α-Ga_2O_3, β-Ga_2O_3, and ε-Ga_2O_3 at 300 K. The temperature dependence of κ values of β-Ga_2O_3 has been plotted [Fig. 3(b)], together with the TDTR measurement [54] and DFT-BTE calculation [20] results. The predictions from other ML potentials based on DeepMD (DP-MD)

have also been included for comparison.[51] The κ values calculated by the NEP were in great agreement with the experimental results and DP-MD predictions in all three directions. However, all of the values were lower than those calculated based on BTE. As a possible reason why the NEP/DP-MD prediction results were both lower than the first-principles calculation results, the BTE method usually truncated the anharmonic force constants to the third order,[55] whereas NEP/DP-MD simulations naturally included higher-order anharmonic force constants,[51] which could thus consider force constants more comprehensively than the BTE method. As mentioned by R. Li et al.,[51] it was really challenging to obtain the thermal conductivity value of β-Ga_2O_3 via BTE method due to the complexity of the β-Ga_2O_3 unit cell and the uncertainties of the convergence process for different parameters. Moreover, it could be found that the κ values of β-Ga_2O_3 calculated by BTE in the [010] and [001] directions in the previous work were nearly the same[20], which were distinct from the experimental results[54], DeepMD results[51], and our results. In summary, it could be found that the previously reported thermal conductivity of β-Ga_2O_3 predicted by the BTE method[20] is slightly higher than the predicted values by the NEP method in our work, which we believe is due to the ignorance of the fourth-order or even higher-order force anharmonic constants in BTE method. Notably, as our calculated values were already in good agreement with the experimental values, the quantum effects have not been taken into account in our calculations. Besides, compared with the quantum statistics, the classical statistics could give a larger modal heat capacities at high frequencies, but smaller phonon scattering times at low frequencies,[55] and in addition, the quantum correction was still controversial in terms of explaining quantum effects.

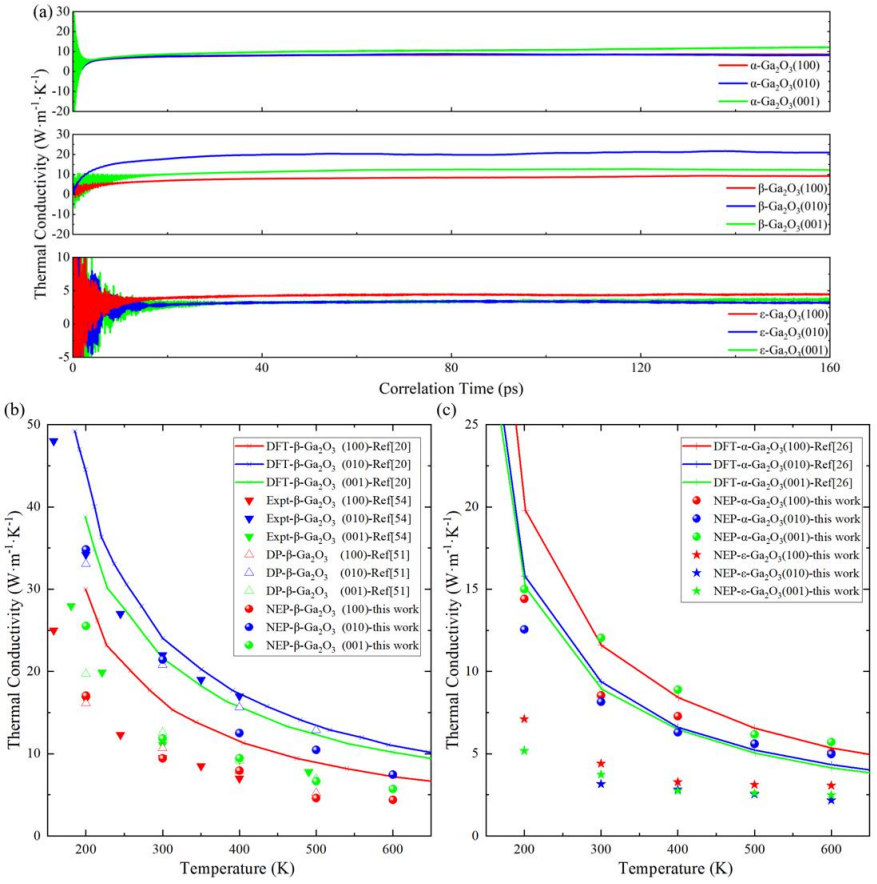

Fig. 3 (a) Thermal conductivity of α-Ga_2O_3, β-Ga_2O_3, and ε-Ga_2O_3 along different crystal orientations at 300K as a function of correlation time using the Green–Kubo method with the NEP, each of which is the average of 50 independent simulations. (b) Temperature-dependent thermal conductivity calculated from NEP- EMD for the different crystal directions of β-Ga_2O_3 (solid circle), compared with the reported experimental values [54] (solid inverted triangle), DFT [20] (solid lines), and DP-MD [51] (hollow triangle). (c) Temperature-dependent thermal conductivity calculated from NEP-EMD for ε-Ga_2O_3 (solid pentagram) and α-Ga_2O_3 (solid circle) compared with the reported DFT [26] (solid lines)

Based on the specific NEP and EMD, the thermal conductivity of the α-Ga_2O_3 and ε- Ga_2O_3 has been calculated. The thermal conductivity of α-Ga_2O_3 in three directions at 300 K was $\kappa_{[100]} = 8.55$, $\kappa_{[010]} = 8.16$, and $\kappa_{[001]} = 12.04$ $W \cdot m^{-1} \cdot K^{-1}$, respectively [Fig. 3 (a)]. These values were basically consistent with $\kappa_{[100]} = 11.61$, $\kappa_{[010]} = 9.38$, and $\kappa_{[001]} = 8.94$ $W \cdot m^{-1} \cdot K^{-1}$ calculated by Vilquin et al. [26] [Fig. 3(c)], while the crystallographic orientation was different. Our calculated values were consistent

in the [100] and [010] directions. Notably, Vilquin's group acquired the same values in the [010] and [001] directions. The unit cell of α-Ga_2O_3 essentially had the same structure in the [100] and [010] directions, whereas in the [001] direction the structure was obviously different [Fig. 1(a)]. Therefore, it could be believed that our calculation results were reliable. One possible reason for the discrepancies between our results and those of Vilquin's group was that they used primitive cells for the calculations, whereas we used conventional unit cells that probably led to differences in the crystal orientation.

The thermal conductivities of ε-Ga_2O_3 in three directions at 300 K were $\kappa_{[100]} = 4.39$, $\kappa_{[010]} = 3.15$, and $\kappa_{[001]} = 3.73$ $W \cdot m^{-1} \cdot K^{-1}$, respectively [Fig. 3(a)]. It could be observed that the thermal conductivity of ε-Ga_2O_3 was significantly lower than that of the α and β phases. The average thermal conductivity [$\kappa_{average} = (\kappa_{100} + \kappa_{010} + \kappa_{001})/3$] of ε-$Ga_2O_3$ at 300 K was 3.76 $W \cdot m^{-1} \cdot K^{-1}$, which was 26.4% that of β-Ga_2O_3 ($\kappa_{[average-\beta]} = 14.25$ $W \cdot m^{-1} \cdot K^{-1}$). Zhou et al. also calculated the thermal conductivity of ε-Ga_2O_3,[27] and claimed that the calculated value they obtained was too large. The thermal conductivity of β-Ga_2O_3 and ε-Ga_2O_3 at 300 K was as high as 41 and 12 $W \cdot m^{-1} \cdot K^{-1}$, respectively. Interestingly, the calculated thermal conductivity of ε-Ga_2O_3 was about 29% that of β-Ga_2O_3, which was consistent with our value of 26.4%. Therefore, it could be indicated that the thermal conductivity value for ε-Ga_2O_3 in our research was probably more accurate. It could also be observed that the anisotropy of ε-Ga_2O_3 was not obvious above 300 K. However, at 200 K, the κ value in the [100] direction was significantly higher than those in the other two crystal directions [Fig. 3(c)].

To evaluate the accuracy of the harmonic force constants for NEP, the phonon dispersion relations along the selected high-symmetry paths and the vibration density of states (VDOS) have been calculated using the primitive cells of each phase [Fig. 1(d-f)]. As ε-Ga_2O_3 has central inversion asymmetry, and the conventional unit cell is also the primitive cell.

The phonon dispersion and VDOS of α-Ga_2O_3, β-Ga_2O_3, and ε-Ga_2O_3 calculated by NEP were in good agreement with the results calculated using the DFT method [Fig. 4]. It could be indicated that the NEP could accurately predict the thermal conductivity of Ga_2O_3. Considering the low symmetry and high anisotropy of Ga_2O_3, it was reasonable that the phonon dispersion in this material was more complicated than that in other UWBG materials, such as GaN or diamond.[23, 56]

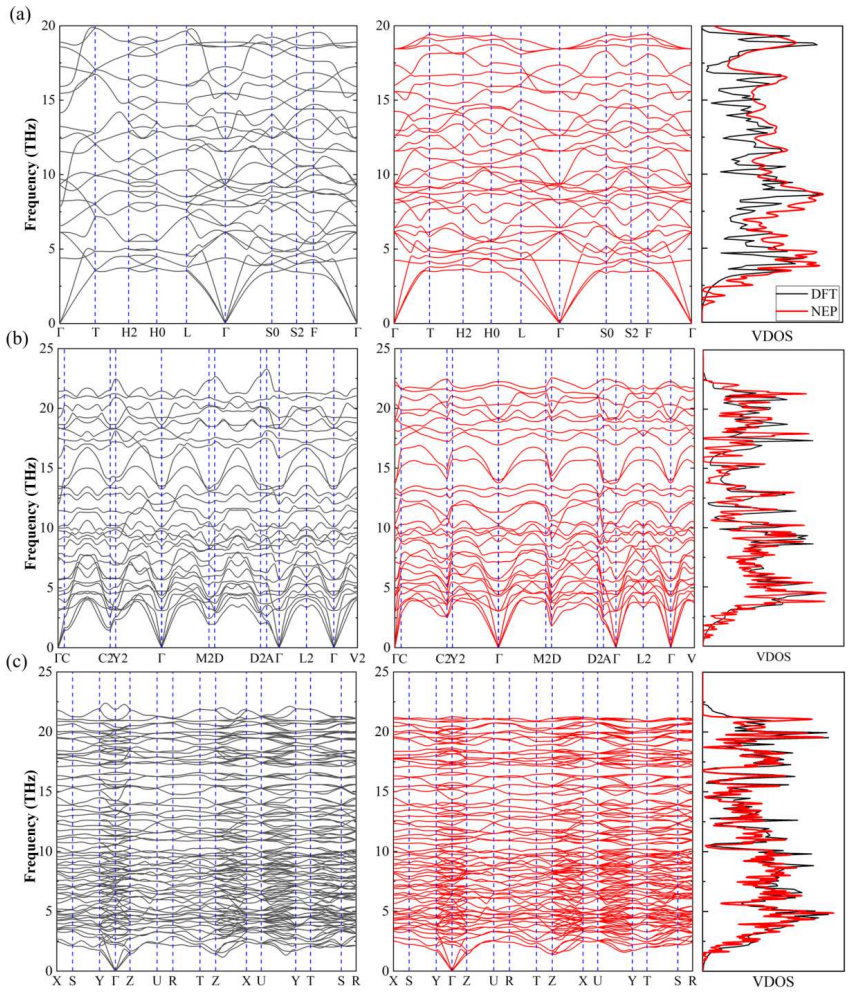

Fig. 4 Phonon dispersion and vibration density of states (VDOS) of (a) α-Ga_2O_3, (b) β-Ga_2O_3, and (c) ε-Ga_2O_3, respectively.

At 300 K, the average thermal conductivities of α-Ga_2O_3, β-Ga_2O_3, and ε-Ga_2O_3 were 9.58, 14.25, and 3.76 $W \cdot m^{-1} \cdot K^{-1}$, respectively. Among them, $\kappa_{[average-\alpha]}$ was 67.2% that of β-Ga_2O_3 and $\kappa_{[average-\varepsilon]}$ was only 26.4% that of β-Ga_2O_3. The large difference between them was worth exploring. Here, the phonon mean free path, the thermal conductivity versus frequency and the participation ratio could be referred to and analyzed in Fig. 5. Overall, the phonon mean free path of β-Ga_2O_3 was the highest among the three phases while the phonon mean free path of ε-Ga_2O_3 was the lowest. We

think this was one of the possible reasons for the $\kappa_{[average-\beta]} > \kappa_{[average-\alpha]} > \kappa_{[average-\varepsilon]}$. As shown in Fig. 5b, the thermal conductivity of Ga_2O_3 was mainly affected by phonons below 10 THz. It could be seen that when the phonon frequency was below 10 THz, the values of participation ratio for Ga_2O_3 phases was in the order of β-Ga_2O_3 > α-Ga_2O_3 > ε-Ga_2O_3 [Fig. 5c], which we think could be another reason for the difference in their thermal conductivities. The [010] direction of β-Ga_2O_3 had the largest coverage of high thermal conductivity contribution phonons (HTCPs) from 0–10 THz [Fig. 5b]. This might lead to the fact that the [010] direction of β-Ga_2O_3 had the highest thermal conductivity. Although the thermal conductivity in [001] direction of α-Ga_2O_3 was not as large as that in the [010] direction of β-Ga_2O_3, it had the highest peak value in the thermal conductivity spectra, which might explain why it could also exhibit excellent thermal conductivity.

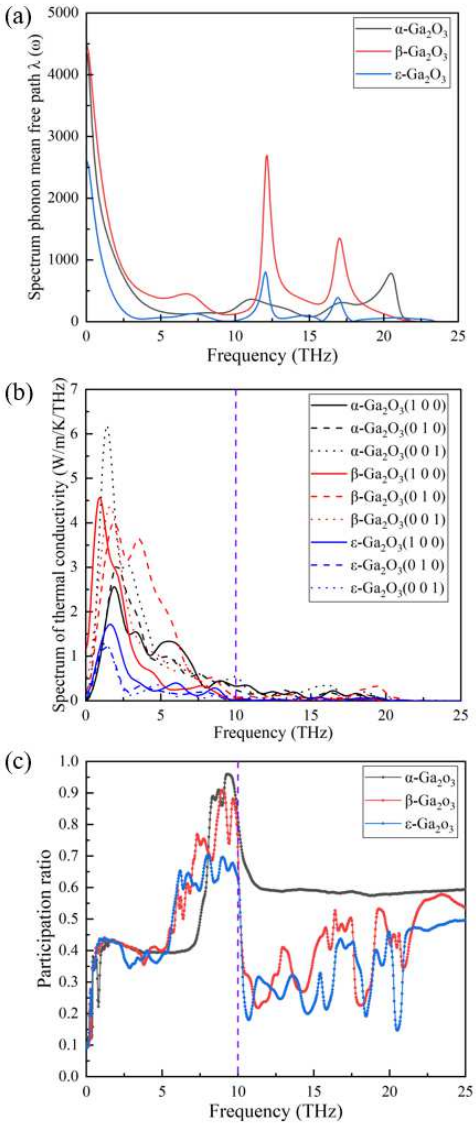

Fig. 5 (a) Spectra phonon mean free path. (b) Thermal conductivity spectra. (c) Participation ratio of α-Ga_2O_3, β-Ga_2O_3, and ε-Ga_2O_3 at 300 K.

At the same time, if the entire conventional unit cell was regarded as a particle that could transmit vibration and heat (all phase blocks were composed of this particle in the same arrangement), it could be inferred that the greater mass of the particle might mean the more energy loss during the

transmitting process, leading to the lower thermal conductivity. The order of the relative atomic mass of the conventional unit cell was as follows: β-Ga_2O_3 < α-Ga_2O_3 < ε-Ga_2O_3. This might also be one of the reasons for $\kappa_{[average-\varepsilon]} < \kappa_{[average-\alpha]} < \kappa_{[average-\beta]}$. Especially, ε-$Ga_2O_3$ had central inversion asymmetry; thus, the symmetry of the unit cell was complicated, which might hinder the heat flow in the unit cell.

In summary, one interatomic potential for Ga_2O_3 polymorphs has been developed using neural networks. The NEP has been trained with ab *initio* energies and forces so that it can generate phonon dispersion and VDOS in good agreement with the DFT results. Based on this NEP, the lattice thermal conductivity of α-Ga_2O_3, β-Ga_2O_3, and ε-Ga_2O_3 at different temperatures has been predicted using EMD. The predicted thermal conductivity values of β-Ga_2O_3 in this work have been proven to be in great agreement with the experimental results as well as the calculated results derived from DP potential. In addition, the predicted thermal conductivity values of α-Ga_2O_3 are also in good agreement with those calculated by other research groups. Thus, on the whole, the accuracy of the proposed NEP in this work can be demonstrated for the prediction of thermal properties of α, β, and ε-Ga_2O_3. On this basis, the thermal conductivity of ε-Ga_2O_3 has been predicted and a reliable value has been achieved, which has not been reported with such high accuracy yet. At 300 K, the predicted values are shown as follows: $\kappa_{[\alpha-100]} = 8.55$, $\kappa_{[\alpha-010]} = 8.16$, and $\kappa_{[\alpha-001]} = 12.04$ $W \cdot m^{-1} \cdot K^{-1}$; $\kappa_{[\beta-100]} = 9.44$, $\kappa_{[\beta-010]} = 21.46$, and $\kappa_{[\beta-001]} = 11.86$ $W \cdot m^{-1} \cdot K^{-1}$; and $\kappa_{[\varepsilon-100]} = 4.39$, $\kappa_{[\varepsilon-010]} = 3.15$, and $\kappa_{[\varepsilon-001]} = 3.73$ $W \cdot m^{-1} \cdot K^{-1}$. In addition, it can be found that $\kappa_{[average-\alpha]}$ is 67.2% that of β-Ga_2O_3, and $\kappa_{[average-\varepsilon]}$ is only 26.4% that of β-Ga_2O_3. By analyzing the phonon dispersion, VDOS, phonon mean free path spectra, participation ratio and thermal conductivity spectra, the reasons for the different thermal conductivities of α-Ga_2O_3, β-Ga_2O_3, and ε-Ga_2O_3 have been explored. Firstly, the narrower HTCPs, lower phonon mean free path and lower participation ratio could indicate that there are fewer phonons effectively contributing to the heat transfer. Secondly, the poor symmetry could be another important factor which may hinder the heat flow in the lattice. Thirdly, the larger number of atoms in the unit cell may also be the reason, which could lead to more energy loss during the cell-to-cell heat transport. In conclusion, a scheme has been proposed in our work for accurately predicting the thermal conductivity of Ga_2O_3 and a relatively accurate value of the thermal conductivity of ε-Ga_2O_3 has been achieved, which could also provide an atomic-scale perspective for the insight into the thermal conductivity differences among α, β, and ε-Ga_2O_3 and further facilitate the development of Ga_2O_3-

based semiconductor devices, especially for the high-power applications.

Supplementary Material

The ***supporting information*** mentioned in this work has been presented in the Supplementary Material, including the schematic presentation of the NEP framework, the details of the training data and the equilibrium molecular dynamics simulation, and the details of the DFT-BTE and DFT-NEP-MD method for the thermal conductivity calculation.

Declaration of Competing Interest

The authors declare no conflict of interest.

Data Availability

The data that support the findings of this study are available from the corresponding author upon reasonable request.

Acknowledgements

This work is funded by the National Natural Science Foundation of China (Grant No. 62004141, 52202045), the Fundamental Research Funds for the Central Universities (Grant No. 2042022kf1028, 2042023kf0112), the Major Program of Hubei Province (Grant No. 2023BAA009), the Knowledge Innovation Program of Wuhan-Shuguang (Grant No. 2023010201020243, 2023010201020255), the Hubei Natural Science Foundation (Grant No. 2022CFB606), and the Open Fund of Hubei Key Laboratory of Electronic Manufacturing and Packaging Integration (Grant No. EMPI2023027).

References

[1]F. Shan, G. Liu, W. Lee, G. Lee, I. Kim, B. Shin, Structural, electrical, and optical properties of transparent gallium oxide

thin films grown by plasma-enhanced atomic layer deposition, Journal of Applied Physics 98(2) 023504. (2005)

[2]J. Tsao, S. Chowdhury, M. Hollis, D. Jena, N. Johnson, K. Jones, R. Kaplar, S. Rajan, C. Van de Walle, E. Bellotti, Ultrawide-bandgap semiconductors: research opportunities and challenges, Advanced Electronic Materials 4(1) 1600501. (2018)

[3]S. Fujita, Wide-bandgap semiconductor materials: For their full bloom, Japanese Journal of Applied Physics 54(3) 030101. (2015)

[4]M. Kim, J.-H. Seo, U. Singisetti, Z. Ma, Recent advances in free-standing single crystalline wide band-gap semiconductors and their applications: GaN, SiC, ZnO, β-Ga_2O_3, and diamond, Journal of Materials Chemistry C 5(33) 8338-8354. (2017)

[5]S. Pearton, J. Yang, P.H. Cary IV, F. Ren, J. Kim, M.J. Tadjer, M.A. Mastro, A review of Ga_2O_3 materials, processing, and devices, Applied Physics Reviews 5(1) 011301. (2018)

[6]Z. Yan, S. Kumar, Phonon mode contributions to thermal conductivity of pristine and defective β-Ga_2O_3, Physical Chemistry Chemical Physics 20(46) 29236-29242. (2018)

[7]H. Wu, S. Ning, N. Qi, F. Ren, Z. Chen, X. Su, X. Tang, Extremely low thermal conductivity of β-Ga_2O_3 with porous structure, Journal of Applied Physics 130(19) 195103. (2021)

[8]R. Roy, V. Hill, E. Osborn, Polymorphism of Ga_2O_3 and the system Ga_2O_3-H_2O, Journal of the American Chemical Society 74(3) 719-722. (1952)

[9]S. Yoshioka, H. Hayashi, A. Kuwabara, F. Oba, K. Matsunaga, I. Tanaka, Structures and energetics of Ga_2O_3 polymorphs, Journal of Physics: Condensed Matter 19(34) 346211. (2007)

[10]K. Kaneko, S. Fujita, T. Hitora, A power device material of corundum-structured α-Ga_2O_3 fabricated by MIST EPITAXY® technique, Japanese Journal of Applied Physics 57(2S2) 02CB18. (2018)

[11]Y. Qin, L. Li, X. Zhao, G.S. Tompa, H. Dong, G. Jian, Q. He, P. Tan, X. Hou, Z. Zhang, Metal–semiconductor–metal ε-Ga_2O_3 solar-blind photodetectors with a record-high responsivity rejection ratio and their gain mechanism, Acs Photonics 7(3) 812-820. (2020)

[12]M. Zhang, Z. Liu, L. Yang, J. Yao, J. Chen, J. Zhang, W. Wei, Y. Guo, W. Tang, β-Ga_2O_3-based power devices: a concise review, Crystals 12(3) 406. (2022)

[13]M. Handwerg, R. Mitdank, Z. Galazka, S. Fischer, Temperature-dependent thermal conductivity and diffusivity of a Mg-doped insulating β-Ga_2O_3 single crystal along [100],[010] and [001], Semiconductor Science and Technology 31(12) 125006. (2016)

[14]M. Handwerg, R. Mitdank, Z. Galazka, S. Fischer, Temperature-dependent thermal conductivity in Mg-doped and undoped β-Ga_2O_3 bulk-crystals, Semiconductor Science and Technology 30(2) 024006. (2015)

[15]Z. Guo, A. Verma, X. Wu, F. Sun, A. Hickman, T. Masui, A. Kuramata, M. Higashiwaki, D. Jena, T. Luo, Anisotropic thermal conductivity in single crystal β-gallium oxide, Applied Physics Letters 106(11) 111909. (2015)

[16]M. Slomski, N. Blumenschein, P. Paskov, J. Muth, T. Paskova, Anisotropic thermal conductivity of β-Ga_2O_3 at elevated temperatures: Effect of Sn and Fe dopants, Journal of Applied Physics 121(23) 235104. (2017)

[17]N. Blumenschein, M. Slomski, P.P. Paskov, F. Kaess, M. Breckenridge, J. Muth, T. Paskova, Thermal conductivity of bulk and thin film [beta]-Ga_2O_3 measured by the 3 [omega] technique, Oxide-based Materials and Devices IX 10533 (2018) 228-235.

[18]Y. Zheng, E. Swinnich, J.-H. Seo, Investigation of thermal properties of β-Ga_2O_3 nanomembranes on diamond heterostructure using Raman thermometry, ECS Journal of Solid State Science and Technology 9(5) 055007. (2020)

[19]Y. Zhang, Q. Su, J. Zhu, S. Koirala, S.J. Koester, X. Wang, Thickness-dependent thermal conductivity of mechanically exfoliated β-Ga_2O_3 thin films, Applied Physics Letters 116(20) 202101. (2020)

[20]M.D. Santia, N. Tandon, J. Albrecht, Lattice thermal conductivity in β-Ga_2O_3 from first principles, Applied Physics Letters 107(4) 041907. (2015)

[21]Z. Gao, Z. Zhang, G. Liu, J.-S. Wang, Ultra-low lattice thermal conductivity of monolayer penta-silicene and penta-germanene, Physical Chemistry Chemical Physics 21(47) 26033-26040. (2019)

[22]G. Qin, M. Hu, Diverse thermal transport properties of two-dimensional materials: a comparative review, TWO-DIMENSIONAL MATERIALS 199. (2016)

[23]L. Shi, X. Ma, M. Li, Y. Zhong, L. Yang, W. Yin, X. He, Molecular dynamics simulation of phonon thermal transport in nanotwinned diamond with a new optimized Tersoff potential, Physical Chemistry Chemical Physics 23(14) 8336-8343. (2021)

[24]Z. Qi, W. Shen, R. Li, X. Sun, L. Li, Q. Wang, G. Wu, K. Liang, AlN/diamond interface nanoengineering for reducing thermal boundary resistance by molecular dynamics simulations, Applied Surface Science 615 156419. (2023)

[25]H. Chen, Q. Nie, H. Fang, Dynamic behavior of droplets on confined porous substrates: A many-body dissipative particle dynamics study, Physics of Fluids 32(10) 102003. (2020)

[26]G. Yang, P.R. Romeo, A. Apostoluk, B. Vilquin, First principles study on the lattice thermal conductivity of α-phase Ga_2O_3, Journal of Vacuum Science & Technology A: Vacuum, Surfaces, and Films 40(5) 052801. (2022)

[27]Q. Liu, Z. Chen, X. Zhou, Electronic, thermal, and thermoelectric transport properties of ε-Ga_2O_3 from first principles, ACS Omega 7(14) 11643-11653. (2022)

[28]H. Bao, J. Chen, X. Gu, B. Cao, A review of simulation methods in micro/nanoscale heat conduction, ES Energy & Environment 1(39) 16-55. (2018)

[29]J.R. Lloyd, T. Luo, Handbook of molecular dynamics potential functions, Begell House, New York, 2011.

[30]X. Wan, W. Feng, Y. Wang, H. Wang, X. Zhang, C. Deng, N. Yang, Materials discovery and properties prediction in thermal transport via materials informatics: a mini review, Nano Lett. 19(6) 3387-3395. (2019)

[31]Z. Fan, Improving the accuracy of the neuroevolution machine learning potential for multi-component systems, Journal of Physics: Condensed Matter 34(12) 125902. (2022)

[32]A.P. Bartók, J. Kermode, N. Bernstein, G. Csányi, Machine learning a general-purpose interatomic potential for silicon, Physical Review X 8(4) 041048. (2018)

[33]X. Qian, R. Yang, Temperature effect on the phonon dispersion stability of zirconium by machine learning driven atomistic simulations, Physical Review B 98(22) 224108. (2018)

[34]P. Rowe, G. Csányi, D. Alfe, A. Michaelides, Development of a machine learning potential for graphene, Physical Review B 97(5) 054303. (2018)

[35]X. Gu, C. Zhao, Thermal conductivity of single-layer $MoS_{2\,(1-x)}\,Se_{2x}$ alloys from molecular dynamics simulations with a machine-learning-based interatomic potential, Computational Materials Science 165 74-81. (2019)

[36]G. Kresse, J. Furthmüller, Efficiency of ab-initio total energy calculations for metals and semiconductors using a plane-wave basis set, Computational Materials Science 6(1) 15-50. (1996)

[37]G. Kresse, D. Joubert, From ultrasoft pseudopotentials to the projector augmented-wave method, Physical Review B 59(3) 1758. (1999)

[38]Z. Fan, W. Chen, V. Vierimaa, A. Harju, Efficient molecular dynamics simulations with many-body potentials on graphics processing units, Computer Physics Communications 218 10-16. (2017)

[39]Z. Fan, T. Siro, A. Harju, Accelerated molecular dynamics force evaluation on graphics processing units for thermal conductivity calculations, Computer Physics Communications 184(5) 1414-1425. (2013)

[40]B. Mortazavi, Z. Fan, L.F.C. Pereira, A. Harju, T. Rabczuk, Amorphized graphene: a stiff material with low thermal conductivity, Carbon 103 318-326. (2016)

[41]H. He, R. Orlando, M.A. Blanco, R. Pandey, E. Amzallag, I. Baraille, M. Rérat, First-principles study of the structural, electronic, and optical properties of Ga_2O_3 in its monoclinic and hexagonal phases, Physical Review B 74(19) 195123. (2006)

[42]J. Åhman, G. Svensson, J. Albertsson, A reinvestigation of β-gallium oxide, Acta Crystallographica Section C: Crystal Structure Communications 52(6) 1336-1338. (1996)

[43]K. Momma, F. Izumi, VESTA 3 for three-dimensional visualization of crystal, volumetric and morphology data, Journal of Applied Crystallography 44(6) 1272-1276. (2011)

[44]S.K. Achar, L. Zhang, J.K. Johnson, Efficiently trained deep learning potential for graphane, The Journal of Physical

Chemistry C 125(27) 14874-14882. (2021)

[45]Z. Fan, Z. Zeng, C. Zhang, Y. Wang, K. Song, H. Dong, Y. Chen, T. Ala-Nissila, Neuroevolution machine learning potentials: Combining high accuracy and low cost in atomistic simulations and application to heat transport, Physical Review B 104(10) 104309. (2021)

[46]Z. Fan, Y. Wang, P. Ying, K. Song, J. Wang, Y. Wang, Z. Zeng, K. Xu, E. Lindgren, J.M. Rahm, GPUMD: A package for constructing accurate machine-learned potentials and performing highly efficient atomistic simulations, The Journal of Chemical Physics 157(11). (2022)

[47]R. Kubo, M. Toda, N. Hashitsume, Statistical physics II: nonequilibrium statistical mechanics, Springer Science & Business Media, Berlin, 2012.

[48]H. Meng, X. Yu, H. Feng, Z. Xue, N. Yang, Superior thermal conductivity of poly (ethylene oxide) for solid-state electrolytes: A molecular dynamics study, International Journal of Heat and Mass Transfer 137 1241-1246. (2019)

[49]X. Yu, R. Li, T. Shiga, L. Feng, M. An, L. Zhang, J. Shiomi, N. Yang, Hybrid thermal transport characteristics of doped organic semiconductor poly (3, 4-ethylenedioxythiophene): tosylate, The Journal of Physical Chemistry C 123(43) 26735-26741. (2019)

[50]R. Kubo, Statistical-mechanical theory of irreversible processes. I. General theory and simple applications to magnetic and conduction problems, Journal of the Physical Society of Japan 12(6) 570-586. (1957)

[51]R. Li, Z. Liu, A. Rohskopf, K. Gordiz, A. Henry, E. Lee, T. Luo, A deep neural network interatomic potential for studying thermal conductivity of β-Ga_2O_3, Applied Physics Letters 117(15) 152102. (2020)

[52]Y.-B. Liu, J.-Y. Yang, G.-M. Xin, L.-H. Liu, G. Csányi, B.-Y. Cao, Machine learning interatomic potential developed for molecular simulations on thermal properties of β-Ga_2O_3, The Journal of Chemical Physics 153(14) 144501. (2020)

[53]H. Yanxon, D. Zagaceta, B. Tang, D.S. Matteson, Q. Zhu, PyXtal_FF: a python library for automated force field generation, Machine Learning: Science and Technology 2(2) 027001. (2020)

[54]P. Jiang, X. Qian, X. Li, R. Yang, Three-dimensional anisotropic thermal conductivity tensor of single crystalline β-Ga_2O_3, Applied Physics Letters 113(23) 232105. (2018)

[55]T. Feng, L. Lindsay, X. Ruan, Four-phonon scattering significantly reduces intrinsic thermal conductivity of solids, Physical Review B 96(16) 161201. (2017)

[56]X. Wu, J. Lee, V. Varshney, J.L. Wohlwend, A.K. Roy, T. Luo, Thermal conductivity of wurtzite zinc-oxide from first-principles lattice dynamics–a comparative study with gallium nitride, Scientific Reports 6(1) 1-10. (2016)